Proceedings of
11th European Conference on Turbomachinery Fluid dynamics & Thermodynamics
ETC11, March 23-27, 2015, Madrid, Spain

ANALYTICAL LOSS PREDICTION FOR TURBOCHARGER COMPRESSORS

M. Schneider - J. Bühler - M. Hanna - H.-P. Schiffer

Technische Universität Darmstadt
Institute of Gas Turbines and Aerospace Propulsion
Otto-Berndt-Straße 2, 64287 Darmstadt, Germany

S. Leichtfuß

Turbo Science
www.turboscience.de
64287 Darmstadt, Germany

ABSTRACT

A tool for performance prediction of automotive turbocharger centrifugal compressors is presented. The code is based on analytical models from literature and includes vaneless compressor inlet, impeller, vaneless diffuser and a volute. The impeller exit flow is modelled using a modified two-zone approach which accounts for the interaction of aerodynamic blockage and diffusion. Thermal and pressure losses inside the impeller are computed using different collections of loss models from open literature. The data are used to evaluate the percentage of individual loss mechanisms on the overall losses. The predicted performance is compared with highly resolved numerical simulations and experiments. A correlation for the minimal boundary of the aerodynamic blockage coefficient at different operating points is derived from the numerical results which serves as input to the analytical model.

Keywords: automotive turbocharger, radial compressor, analytical modelling, performance prediction, loss prediction, two-zone model

NOMENCLATURE

Latin

A	area (m^2)
C	absolute velocity (m/s)
$DR := W_1/W_{2,jet}$	diffusion ratio
Ma	Mach number
N	rotational speed (RPM)
R	radius (m)
$Ro := h + W^2/2 - U^2/2$	rothalpy (J/kg)
T	static temperature (K)
U	rotational speed (m/s)
W	relative velocity (m/s)
Z	number of blades
$f(\,)$	generic function
h	specific enthalpy (J/kg)
i_{crit}	critical incidence angle $(^\circ)$
k	non-dimensional surface roughness
$\dot{m}$	mass flow (kg/s)
p	static pressure (Pa)
s	specific entropy $(J/(kgK))$
y^+	non-dimensional wall distance
z	axial coordinate (m)

Greek

$\Delta(\,)$	finite difference
$\Pi = p_8/p_0$	pressure ratio
Φ	generic physical quantity
α	absolute flow angle to meridional $(^\circ)$
β	relative flow angle to meridional $(^\circ)$
$\varepsilon := A_{wake}/A$	wake width
η	isentropic efficiency
θ	circumferential coordinate (m)
$\lambda := \Delta h_t/U_2^2$	work or loss coefficient
μ	dynamic viscosity $(kg/(ms))$
$\nu := W_{wake}/W_{jet}$	velocity ratio
ρ	mass density (kg/m^3)
$\sigma := 1 - \Delta C_{2,u}/U_2$	slip factor
$\varphi_2 := C_{2,m}/U_2$	tip flow coefficient
$\chi := \dot{m}_{wake}/\dot{m}_{jet}$	mass flow ratio

Superscripts

$\overline{\square}$	average
$\square'$	relative frame of reference
$\square^*$	sonic state

Subscripts			
		ext	external
		i	ideal
		int	internal
0	initial value	min	minimal
1	inducer	mix	mixed-out state
2	impeller exit	mod	modelled
5	VLD exit	red	reduced
8	volute exit	t	total
∞	ideal case	u	circumferential direction
b	blade	VLD	vaneless diffuser

INTRODUCTION

The increase in emission restrictions and the demand for fuel economy is driving the trend in downsizing automobile engines. In this context highly adapted turbochargers gain significant importance. In order to contribute to this development, an analytical loss prediction tool for radial compressors is implemented at the *Institute of Gas Turbines and Aerospace Propulsion* (GLR) at *Technische Universität Darmstadt*. Thus, a reliable prediction of performance and the composition of losses shall guide the early stages of future developments. The prediction of performance and thermodynamic efficiency of automotive turbocharger compressors is a major application of modern computational fluid dynamics (CFD) solvers which allow a detailed insight and understanding of flow phenomena. However, a major drawback of CFD, when it comes to the applicability to parameter studies in the design process, is the time-consuming adaptation of the numerical grids and the actual computation time. Also, the simulation of entire performance maps is a challenging task due to complex flow structures which are dependent on the respective design and the interaction of the different compressor elements. That is, why the application of computer codes based on simple 1D analytical models may provide a fast reduction of design space before a full 3D CFD simulation of the detailed geometry is run. Drawbacks of the modelling approach are increased uncertainties due to the simplicity of the used correlations and their dependence on empirical parameters as well as the comparably small amount of data that modelling tools are able to provide.

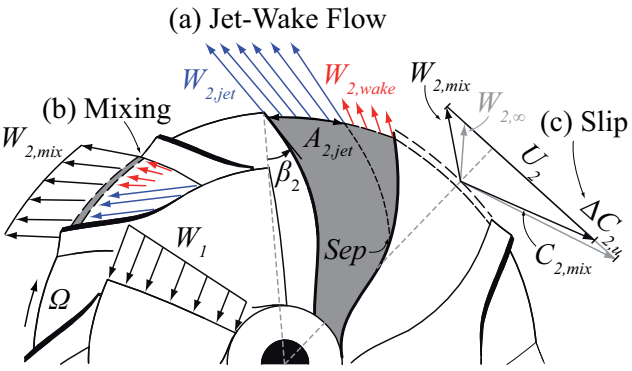

Figure 1: **Impeller Exit Flow Modelling**

The underlying models have a long history of continuous usage and improvement which is the key element to their applicability to a large number of geometrical variations at acceptable errors. Full sets of 1D correlations which enable the loss prediction of radial compressors were published in collections by Galvas [1974], Aungier [1995] and Oh et al. [1997], among others. Analytical models may be classified, as done by Harley et al. [2013], by the number of zones in the modelled flow. *Single-zone* models assume a uniform state perpendicular to a mean streamline. *Two-zone* models split the flow domain according to the jet-wake flow theory by Dean and Senoo [1960] (Figure 1 a). The idea is to assume an isentropic high momentum *jet*-zone within an impeller passage, and account for losses only in the low momentum *wake*. This approach better represents the observable flow phenomena in most impeller geometries but requires the introduction of additional parameters to account for the differences in momentum between the zones.

Performance map limits are usually detected by comparing certain flow parameters to experimentally determined thresholds. Japikse [1984] proposes a correlation for a critical incidence angle $i_{crit} = f(Ma'_1)$ determining the onset of stall. Aungier [1995] uses the equivalent diffusion fac-

tor for the detection of recirculation-induced stall and Harley et al. [2013] use the diffusion ratio for stall detection. The effect of choking on performance can be accounted for by a choke loss (Aungier [1995]) which is triggered if the effective throat area exceeds the critical throat area A^* as defined by Dixon [1998]. The method assumes choking at the geometrically smallest cross-section, which is usually located at the inducer or splitter leading edge, and requires a priori knowledge of the effective flow area at this position.
All prediction models have in common that a realistic estimation of the diffusion across the rotor is required. A common parameter providing this quantity is the diffusion ratio DR. The estimation must take into account the separation of flow in an impeller passage. Separation is enforced by the Coriolis effects due to the relative motion in the impeller channel and tip clearance flows. Japikse [1996] introduced an approach for the off-design modelling of DR according to his *two-elements-in-series* (TEIS) theory.
A speciality of two-zone models is the need to additionally model the momentum of the wake zone which is considered relative to the jet flow by an empirical parameter χ in the original model. The use of a velocity ratio ν rather than the mass flow ratio χ is proposed by van den Braembussche [2013]. He also abandons the assumption of an isentropic jet and introduces an explicit consideration of pressure loss in the jet flow. An advantage of the use of ν rather than χ is the possibility to compute the area ratio of jet and wake flow ε_2 at the impeller exit from continuity, rather than using empirical correlations of the form $\varepsilon_2 = f(\chi_2)$ as done by Oh. et al. [2002]. The idea to limit this parameter to a minimal value $\varepsilon_{2,min}$, accounting for blockage from separated boundary layers and tip clearance flow, is adopted by van den Braembussche [2013] and constitutes the central part of the model presented in the following. A contribution of this work is the provision of an estimation of the form

$$\varepsilon_{2,min} = f(N), \tag{1}$$

which is derived from CFD simulations of an existing turbocharger impeller geometry.

MODELLING

Overall Compressor Model An analytical model is set up as a successive combination of sub-models for inlet, unshrouded impeller, vaneless diffuser (VLD) and volute. All compressor elements are simulated in a procedure without any backward loops, i.e. upstream interaction of the elements on one another is not considered. However, especially the exit volute may have an upstream effect on impeller and diffuser which is captured by *rotor-response* models (van den Braembussche et al. [1999]). The sub-models for the respective components are presented in the following.

Impeller - Overall Structure of the Procedure In the results shown in this work, a mass flow range between 0 and $0.3\,kg/s$ is analysed in discrete steps of $\Delta\dot{m} = 0.015\,kg/s$ for a range of rotational speeds. The choice of $\Delta\dot{m}$ is dependent on geometry and particularly important for the detection of performance map limits as these can only be resolved with the chosen step size.
The impeller exit flow is computed from a two-zone model as proposed by van den Braembussche [2013]. Basic assumptions are the conservation of rothalpy Ro, equal impeller exit flow angles β_2 and mean pressures $\overline{p_2}$ in jet and wake,

$$Ro_1 = Ro_{2,jet} = Ro_{2,wake}, \tag{2}$$
$$\beta_2 = \beta_{2,jet} = \beta_{2,wake} \text{ and} \tag{3}$$
$$\overline{p_2} = \overline{p_{2,jet}} = \overline{p_{2,wake}}, \tag{4}$$

which allow the computation of the impeller exit thermodynamic quantities if the discharge velocities of jet and wake are known. These are estimated from the empirical parameters DR and ν.
Due to the non-linearity of the underlying equations the code consists of an outer loop, that is run for each operating condition. A flowchart of the structure is shown in Figure 3. The outer loop acts as a

closure to the problem so that the slip factor σ is converged. That is, an initial exit flow angle $\beta_{2,0}$ is guessed and iteratively increased until the slip factor σ, computed from the impeller discharge quantities, equals the slip factor σ_{mod} predicted by a model. Equality is assumed within a finite interval of $|\sigma - \sigma_{mod}|/\sigma_{mod} = 0.01$. The exit flow angle is increased in steps of $\Delta\beta = 0.3°$.
A nested inner loop accounts for aerodynamic blockage of the impeller channel and adjusts the impeller exit flow quantities by a gradual increase of $W_{2,jet}$ in steps of $\Delta W_{2,jet} = 0.5\,m/s$. The procedure is described in detail in the next paragraph. The increments in mass flow, flow angle and jet velocity are determined from a refinement study so that their numerical effect on the result is negligible.

Impeller - Blockage Modelling The core element of the inner loop is the computation of the wake blockage coefficient

$$\varepsilon_2 = \frac{\frac{\dot{m}}{A_2 \cos(\beta_2)} - \rho_{2,jet} W_{2,jet}}{\rho_{2,wake} W_{2,wake} - \rho_{2,jet} W_{2,jet}} \tag{5}$$

from mass conservation in the jet-wake structure. The blockage ε_2 may be directly computed for an assumed value of β_2 using the input values for DR and ν to calculate the exit velocities.
It can be shown that for a steadily increasing mass flow rate the value of ε_2 will steadily decrease and finally drop to zero. The idea of the inner loop is to prescribe a *minimal* finite blockage $\varepsilon_{2,min}$ of the impeller trailing edge area, as a certain amount of the outlet cross-section is always blocked by separated and tip leakage cross flow. Thus, the model allows the flow to react to an increase in mass flow at constant rotational speed by an expansion of the jet zone only until it has reached a critical maximum area. Above this limit, more mass inflow leads to an acceleration rather than a widening of the jet, decreasing static pressure rise in the jet zone and thus leading to a descent of the performance curve.
Therefore, if mass flow is increased above a critical value, the computation of ε_2 is iterated in an inner loop (blue in Figures 2 and 3) in order to satisfy the *minimal blockage condition*

$$\varepsilon_2 \geq \varepsilon_{2,min}. \tag{6}$$

That is, an initial guess for the diffusion ratio, DR_0, is used to compute an initial guess for the blockage, $\varepsilon_{2,0}$. If this value is smaller than a prescribed minimal value $\varepsilon_{2,min}$, the diffusion ratio is successively reduced until condition (6) is fulfilled yielding the final values DR and ε_2. At operating conditions where $\varepsilon_{2,0} \geq \varepsilon_{2,min}$ the code does not enter the inner loop, i.e. no adjustments to the diffusion ratio are made and only the outer loop is run until the slip factor is converged. The two cases are illustrated in Figure 2.

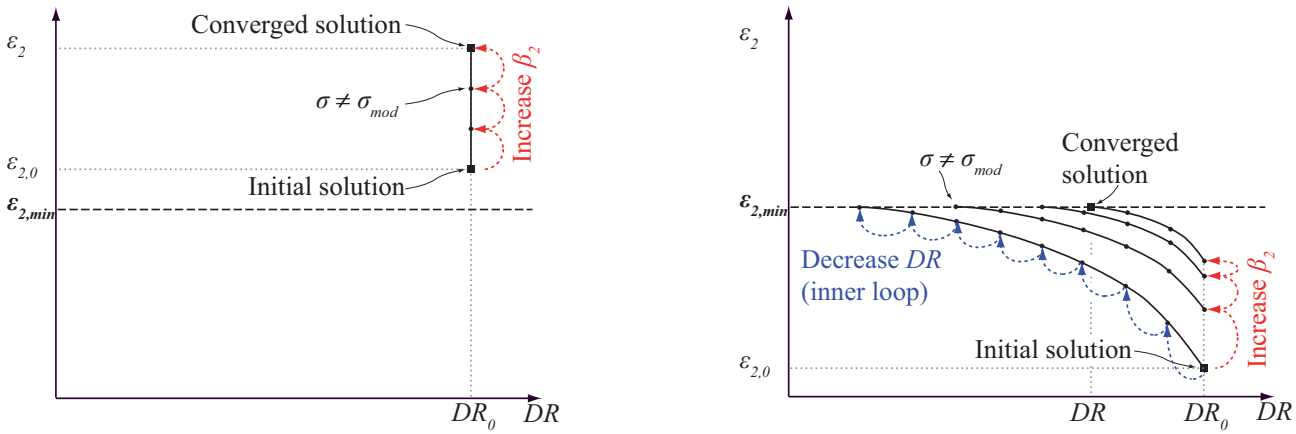

(a) Operation Points for which $\varepsilon_{2,0} \geq \varepsilon_{2,min}$

(b) Operation Points for which $\varepsilon_{2,0} < \varepsilon_{2,min}$

Figure 2: **Illustration of the Iterative Parameter Variations for the Impeller Computation**

The initial diffusion ratio DR_0 is obtained using the TEIS model by Japikse [1996] at zero mass flow, assuming medium efficiency of both elements. However, to the author's knowledge no general analytical model has been published providing a *minimum boundary* for impeller blockage, $\varepsilon_{2,min}$. Therefore, a CFD analysis of an industrial turbocharger impeller was conducted to extract this quantity.

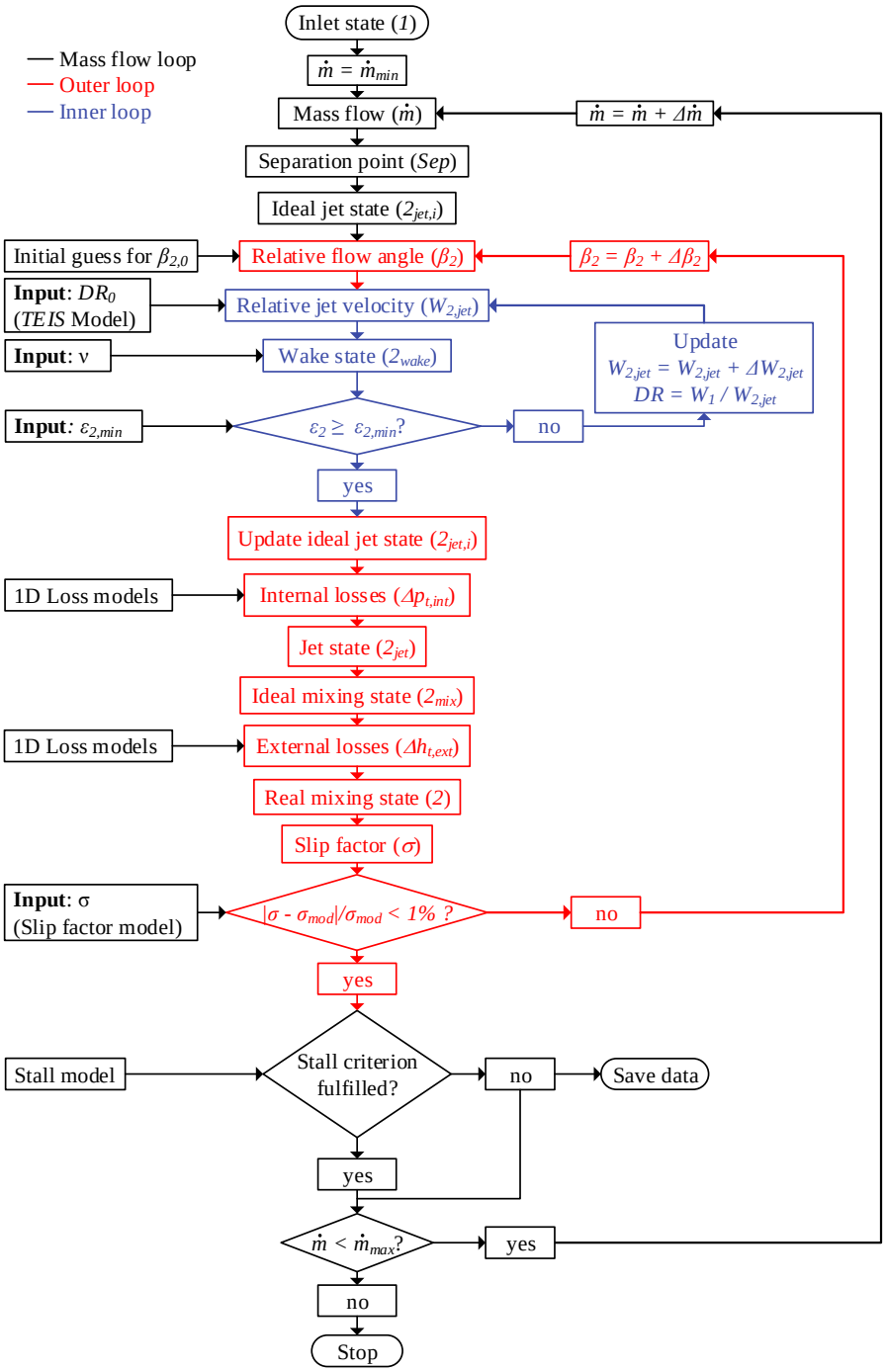

Figure 3: **Flowchart of Impeller Exit Flow Computation**

The applied method has two main advantages. Only a single input value for the diffusion ratio DR_0 is required, instead of a full off-design prediction of DR, and no empirical correlation of the form $\varepsilon_2 = f(\chi_2)$ is needed. Also, the approach provides an inherent modelling of the choke limit as the reduction of DR leads to an increase of $Ma'_{2,jet}$. This can be beneficial as the geometric impeller

outlet cross-section area can usually be determined more accurately than the impeller throat area. On the other hand, an additional input parameter $\varepsilon_{2,min}$ needs to be prescribed at all operation points. Also, the model works well only if choking occurs at the impeller exit rather than the impeller throat cross-section.

Impeller - Losses Impeller losses are computed from 1D correlations in open literature. Losses are distinguished as internal and external according to their effect on the thermodynamic process. *Internal* losses act as total pressure losses Δp_t and are assumed to act on the jet flow only, as it is the portion of the flow carrying energy and increasing the pressure ratio across the impeller. *External* losses account for work input which is not converted into pressure and thus acts as increase in total enthalpy Δh_t. These are applied to a mixed-out state of jet and wake flow which is described below. The loss mechanisms accounted for vary between the different loss collections. Losses included in the collections by Aungier [1995] and Oh et al. [1997] can be seen in Figure 9.
The modelled thermodynamic states are displayed in the diagram in Figure 4. The flow is assumed isentropic until the separation point is reached, where it splits up into jet and wake flow. The isentropic jet state $\Phi_{2,jet,i}$ is mainly determined by the diffusion ratio DR, whereas the wake state $\Phi_{2,wake}$ is determined by the velocity ratio ν. Internal pressure losses $\Delta p_{t,int}$ from loss models yield the final state of the jet $\Phi_{2,jet}$ which mixes with the wake to the effective state $\Phi_{2,mix}$. External losses cause a rise in total enthalpy $\Delta h_{t,ext}$ at constant pressure to the impeller exit state Φ_2. The vaneless diffuser and volute are considered adiabatic thus only causing a further loss in total pressure to the final exit state of the compressor 8.
When comparing the total states in the diagram in Figure 4, it is important to note, that the total pressure of the wake is only higher than that of the jet in an absolute frame of reference ($\circ$). In a relative frame, rotating with the angular velocity of the impeller Ω, total pressure is much higher in the jet ($\diamond$). That is, why the entropy s should be used in order to characterise the wake zone in CFD results as it is independent on the frame of reference (Figure 6 b).
Due to historical reasons the output of loss collections is usually a head loss which is equivalent to a decrement in total enthalpy Δh_t. For the application as internal loss it is converted to total pressure decrement assuming the relation $\Delta h_t = \Delta p_t / \rho$ for incompressible flows. At high rotational speeds, this relation is corrected by a compressibility factor introduced by Aungier [1995].

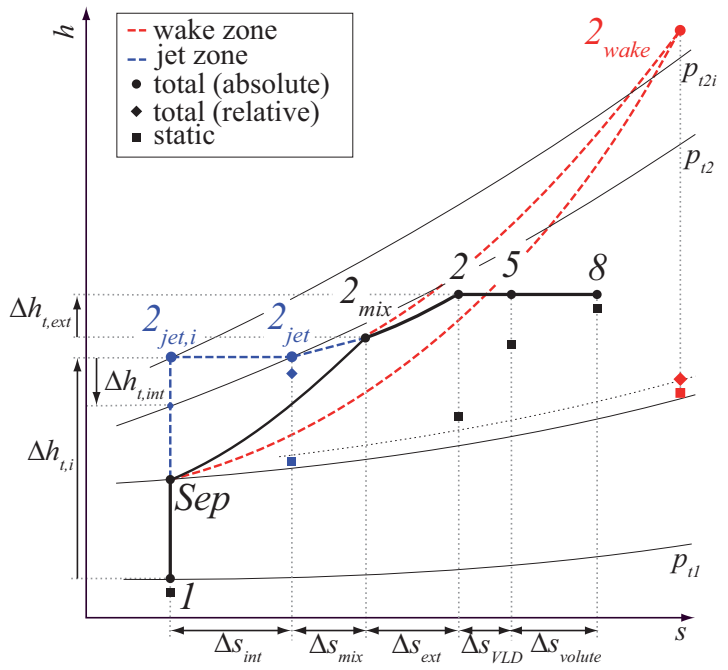

Figure 4: **Diagram of all Modelled States**

Impeller - Exit Mixing, Slip and Stall Exit mixing losses are computed from a mixing calculation at the impeller exit, as suggested by Japikse [1996]. That is, conservation equations for mass, momentum and energy are solved in an infinitesimal control volume directly at the impeller exit (Figure 1 b), yielding an effective mixed out state at the discharge. Mixing losses are then defined as difference between this effective state $\Phi_{2,mix}$ and the mass average of jet and wake at the exit.
The slip factor σ accounts for the slip of absolute circumferential velocity $\Delta C_{2,u}$ at the impeller trailing edge due to Coriolis effects in the impeller passage (Figure 1 c). A value of $\sigma = 1$ corresponds to an ideal flow perfectly guided by the impeller blades[1] with $\beta_{2,\infty} = \beta_{2,b}$. Slip is modelled using the approach by Wiesner [1967], $\sigma = 1 - \sqrt{\cos(\beta_{2,b})}/Z^{0.7}$, and compared with the effective mixed-out state. Thus, the slip factor serves as closure to the iterative numerical procedure as displayed in the flow chart in Figure 3. Stall is detected from the models by Japikse [1984] and Aungier [1995] using the more critical one at each performance curve.

Vaneless Diffuser and Volute The VLD is modelled according to an approach by Stanitz [1952] assuming a compressible 1D flow of the mixed-out fluid through the vaneless space which is subject to friction at the diffuser walls. The model combines the conservation equations for mass, momentum and energy into three ordinary differential equations for Ma, α and T_t. These are numerically integrated to obtain the 1D flow field in the diffuser and the inlet conditions to the volute Φ_5. Heat flux through the diffuser walls is neglected in this work, i.e. $T_t = const.$ in the VLD.
The losses in the volute spiral are obtained from the model by Weber and Koronowski [1986] that evaluates the through flow velocity at the spiral inlet and outlet as well as at the *50 % collection point* which is the circumferential location where $50\,\%$ of the total mass flow has entered the volute. The model assumes the dissipation of the entire meridional component of kinetic energy (meridional velocity dump loss, MVD) and the partial dissipation of the through flow component in the case of flow deceleration in the volute (tangential velocity dump loss, TVD). The ratio of both loss mechanisms depends on the point of operation (Figure 5). Mean flow velocities at the respective cross-sections are computed from the assumption of conservation of tangential momentum $RC_u = const.$ and incompressible flow. Circumferential variations of the inflow conditions Φ_5 and impeller and diffuser response to these variations are not captured by the model.

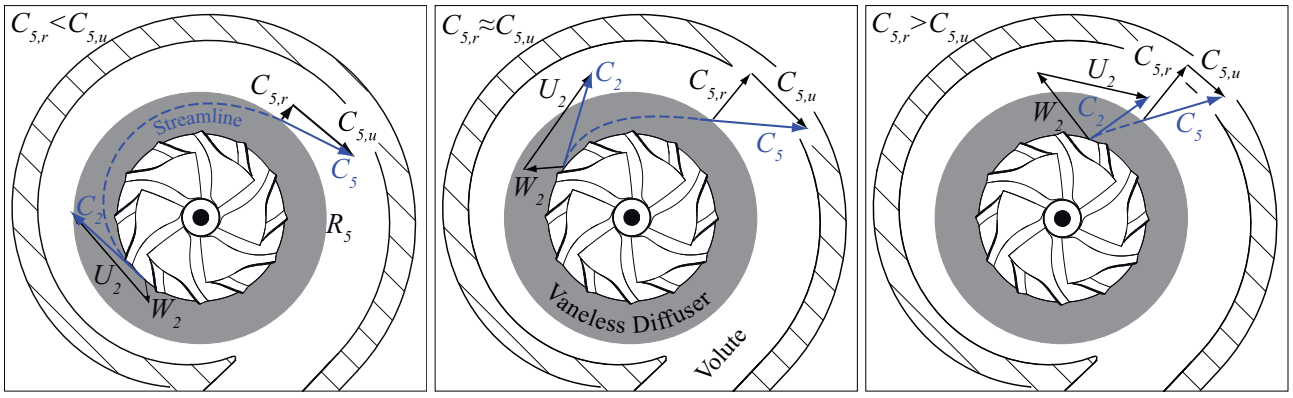

(a) Low Flow Rate (b) Medium Flow Rate (c) High Flow Rate

Figure 5: **Variation of Diffuser and Volute Losses with Mass Flow Rate**

NUMERICAL REFERENCE DATA

Setup of Simulations CFD reference simulations of the analysed geometry are set up according to the data in Table 1 and run at four different constant N_{red} using commercial software. The impeller grid is created structured and then merged with the unstructured volute mesh. In all simulations a

[1] As this case corresponds to a hypothetical geometry with an infinite number of blades, it is denoted by ∞.

mixing-plane after the impeller is utilized to reduce the number of grid cells by simulating only one impeller passage (Figure 6 a).

Table 1: Setup of CFD Simulations

Meshing	Impeller	Volute	**Setup of Simulations**	
Meshing Software	NUMECA AutoGrid5™	NUMECA Hexpress™	Solver	NUMECA FINE™/Open
Mesh type	structured	unstructured	Geometry	single impeller passage
Number of cells	$2.5\,M$	$2.0\,M$		with mixing plane
Min. orthogonality	$24.0°$	$30.9°$	Flow	steady, air (perfect gas)
Max. aspect ratio	2882	515	Boundaries	adiabatic walls
Max. expansion ratio	2.9	3.8	Turbulence	Spalart-Allmaras
Max. y^+	3.0	1.5		(no wall functions)

Extraction of Model Parameters The model input parameters are extracted from CFD simulations by analysing the impeller trailing edge profiles. The quantities of each grid cell $\Phi_2(\theta, z)$ are assigned to the jet zone, if the condition

$$s_2(\theta, z) < \overline{s_2} \tag{7}$$

is fulfilled, and to the wake zone otherwise. The threshold level $\overline{s_2}$, defined as mass average of entropy over the impeller discharge plane at a given operation point, is visualised as a red line in Figure 6 (b). This definition of the jet and wake zone is arbitrary, however, the extracted flow data show to be not very sensitive to variations of $\overline{s_2}$ due to the large entropy gradient between the two zones. The scalar quantities gained from the averaging, $\overline{\Phi_{2,jet}}$ and $\overline{\Phi_{2,wake}}$, are used to derive reference values for the input parameters to the analytical model as shown in Figure 7. The diffusion ratios determined from modelling and CFD are based on the same relative inlet velocity W_1.

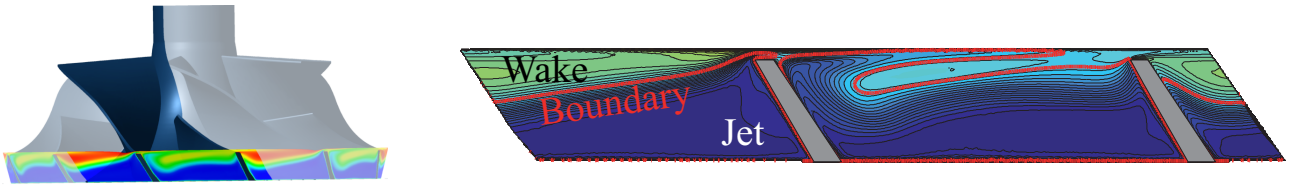

(a) Periodic Impeller Domain

(b) Separation of Impeller Exit Quantities into Jet and Wake Zone

Figure 6: **Jet and Wake Distinction from Entropy Contours**

EXPERIMENTAL REFERENCE DATA

Reference measurements were performed on an open loop radial compressor test rig at GLR. In this experimental setup the turbine and the radial compressor are aerodynamically decoupled. A screw-type compressor and a flow heater ensure the power supply for the turbine. The steady state compressor characteristics are performed at turbine inlet temperatures of $T = 573\,K$ and a maximum inlet mass flow of $\dot{m} = 0.3\,kg/s$. The compressor measurement instrumentation is mounted to fixed measuring planes in order to guarantee high repeatability and to provide comparability between different compressor settings. The total pressure is computed from the measured static and dynamic portions of the flow. The uncertainty of mass flow determination depends on the operating point of the compressor and ranges from $0.7\,\%$ to $0.9\,\%$ of the measured value. For pressure measurements high accuracy pressure transducers and periodically calibrated thermocouples are used. The rotational speed measurements are performed at the turbine wheel to minimize the influence of the instrumentation on the compressor characteristics. The test facility enables online monitoring of all measurement

values as well as the thermodynamic condition of the turbocharger. Therefore, the overall compressor characteristics can be evaluated and it is possible to provide steady condition criteria. In addition unsteady and critical operating conditions are captured and counteracted by pneumatic control devices. In the experimental runs the stability limit is detected from compressor noise. Choke is assumed when efficiency drops below a limiting value.

MODELLING RESULTS

Input Parameters and Sensitivity Study In the analytical model, for increasing mass flow the diffusion ratio DR is fixed at the constant value DR_0 as long as the aerodynamic blockage coefficient ε_2 is decreasing to its minimal value $\varepsilon_{2,min}$. For a further increase of mass flow ε_2 is fixed and DR decreases until the choke limit is reached at $Ma'_{2,jet} = 1$ (Figure 7 a, b).
In order to extract an empirical correlation of wake blockage $\varepsilon_{2,min}(N_{red})$ for the model, the wake blockage ε_2 is computed from CFD at a number of operating conditions (Figure 7 b, □) and the minimal value at a given N_{red} serves as an estimation of $\varepsilon_{2,min}$. In the modelling of the given compressor a linear increase of $\varepsilon_{2,min}$ with N_{red} is assumed from 0.25 to 0.50 (Figure 7 b) corresponding to the range of rotational speeds N in Table 2.
Regarding the data in Figure 7 it is emphasised that the minimal blockage coefficient $\varepsilon_{2,min}$ is the only input parameter that is derived from CFD simulations. The diffusion ratio DR and slip factor σ are shown only for comparison between modelling and CFD results.

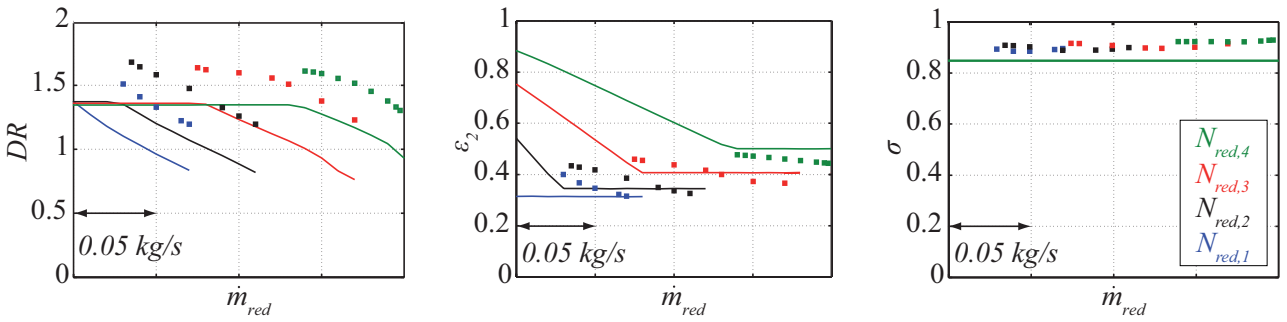

(a) Diffusion Ratio (b) Blockage Coefficient (c) Slip Factor

Figure 7: **Two-Zone Model Parameters, CFD (□) vs. Model (–)**

The velocity ratio is fixed at the literature value of $\nu = 0.20$ according to van den Braembussche [2013] and is not shown in Figure 7 as it has a weak influence on the predicted performance. An alteration of ν either increases specific wake losses at a decreasing portion of wake mass flow or vice versa and therefore does not greatly affect total wake losses.
It can be seen that the slip factors derived from CFD are fairly constant at all rotational speeds on a higher level than the $\sigma = 0.85$ predicted by the Wiesner model. The seemingly small difference largely affects predicted efficiency as in the peak efficiency point of the analysed geometry a deviation of $10\,\%$ in σ causes a change of about $20\,\%$ in the circumferential velocity $C_{2,u}$ which linearly affects the compressor work calculated from *Euler*'s pump equation. It is therefore crucial to provide an accurate estimation of the slip factor σ in order to determine the compressor efficiency correctly (Figure 8 b). For the shown geometry the over-prediction of slip in the Wiesner model is counteracted by an under-prediction of DR_0 from the TEIS model and a cancellation of errors between these quantities is expected. However, the shrinking rate of DR towards the choke limit is in good agreement between the analytical model and CFD (Figure 7 a).

Discussion of Performance Prediction A comparison of the results of analytical modelling with experiments and CFD of an industrial automotive turbocharger are shown in Figure 8. The model input values and operation point data are summarized in Table 2.

Table 2: Input Parameters and Operation Points

DR_0	ν	$\varepsilon_{2,min}$	σ	$\dot{m}\,(kg/s)$	$N\,(RPM)$	$T_1\,(K)$	$p_1\,(kPa)$	$C_{1,u}\,(m/s)$
1.4	0.2	$0.25 - 0.50$	0.85	$0 - 0.3$	$48000 - 176000$	298	100	0

CFD simulations are conducted at four rotational speeds N_{red}. The reduced choking mass flow determined from CFD is in good agreement with experiments, at an over-predicted total pressure ratio, though. No converged solutions could be obtained towards the stability limit with the numerical setup of Table 1. Mesh refinement, variations of turbulence modelling and the application of a frozen rotor approach did not produce any results at this part of the performance map either, which displays the limitations of CFD in centrifugal compressor performance prediction.

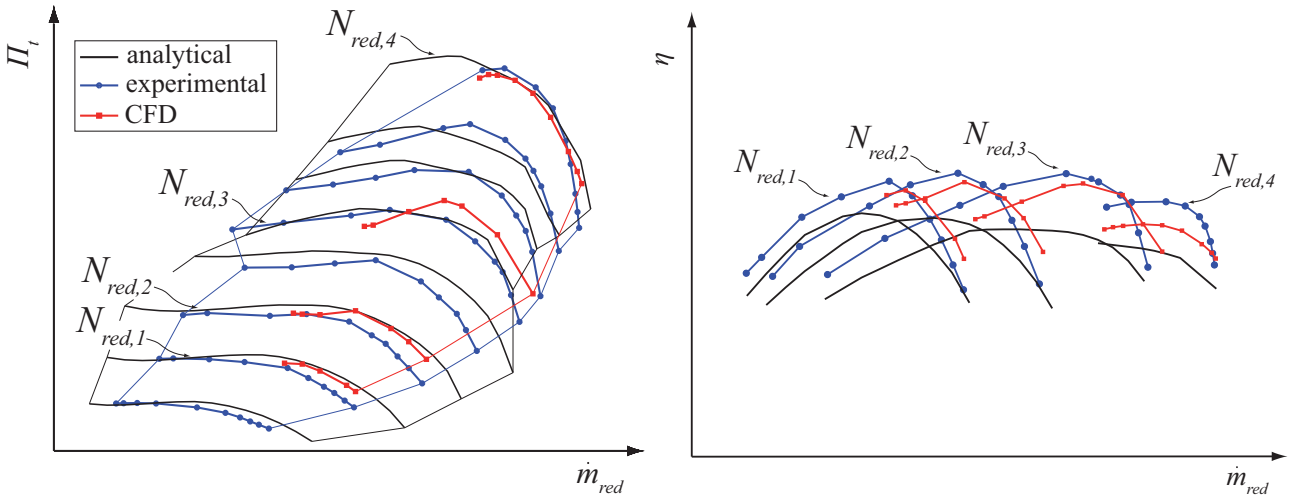

(a) Performance Map

(b) Efficiency Map

Figure 8: **Predicted and Measured Performance**

The analytical model is able to provide an estimation of both performance map limits at all rotational speeds. The detection of the choke limit fits experimental and numerical results best at high rotational speeds. At low speeds there is a considerable divergence of the predicted choke limits. This is expected to occur due to the assumption of choking at the impeller trailing edge in the model. This assumption is found to be fully justified only at high rotational speeds from CFD results.
The detection of stall is achieved by applying two criteria by Aungier [1995] and Japikse [1984] of which the latter one shows to be critical for the given geometry over the whole range of rotational speeds. In order to keep the analytical model applicable to variations of the impeller geometry, the model coefficients, which have been calibrated to a large number of designs, are not fitted to the measured performance map. This results in an offset of the modelled stability limit from experiments at low and high rotational speeds.
The level of the overall modelled pressure rise Π_t is mainly determined by the diffusion ratio DR. Along a performance line this quantity is constant at DR_0 until $\varepsilon_2 = \varepsilon_{2,min}$ and then steadily decreased (Figure 7 a). DR_0 is computed from the TEIS model with efficiencies at a medium level and not adjusted to the experimental data, similar to the stall model coefficients. Thus, the predicted pressure ratio is not in good agreement with experiments at all performance lines. However, the achieved accuracy is of the same order as that of the CFD results and estimated sufficient for a preliminary design analysis.
From the efficiency map in Figure 8 (b) it can be seen that compressor efficiency is predicted only qualitatively correctly at low speeds from the model. There is an offset between experimentally determined and modelled curves increasing with N_{red}, which is at the order of 10 to 15 %. The main

cause of this error is expected to be a wrong prediction of slip by the used empirical correlation which increases with speed (Figure 7 c). A large number of slip factor models is available in literature (Japikse [1996]). However, as none of the published slip models matches the CFD predictions and according to Cumpsty [2004] "in the absence of anything better this is probably the best expression to use" the standard Wiesner model was chosen in the analysis. The unsatisfactory modelling of slip is a well-known issue and a significant improvement of efficiency prediction is expected to be achieved only by a more accurate slip factor prediction.

Discussion of Loss Stack-Ups The model is used to create stack-ups of the non-dimensional loss coefficients λ of the different loss mechanisms at $N_{red,3}$ (Figure 9) similar to the work by Harley et al. [2013]. The straight dashed line which is marked as *ideal* corresponds to an ideal compressor without losses and slip. Considering trailing edge slip yields the red, more realistic performance curve. To this curve the additional work is added which is necessary to compensate for external losses and work lost due to internal losses is subtracted yielding the upper and lower limits of the diagrams. These correspond to work input and output, respectively.

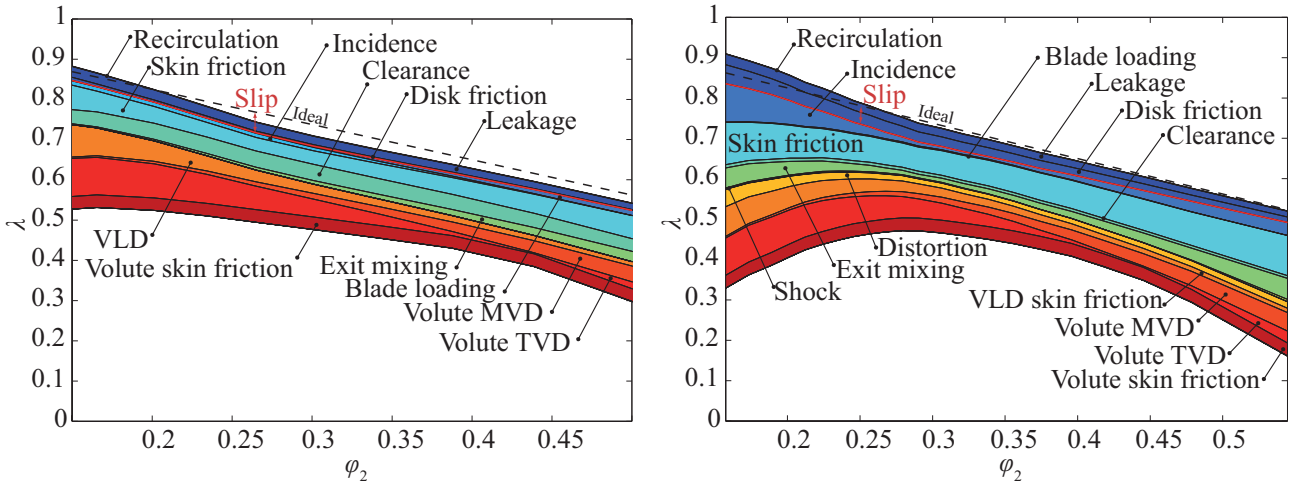

(a) Loss Models by Oh et al. [1997]

(b) Loss Models by Aungier [1995]

Figure 9: **Stack-up of Loss Coefficients vs. Flow Coefficient**

The composition of impeller losses is similar in both loss collections, with the largest differences in the clearance, incidence and exit mixing losses. A detailed comparison of the used loss collections is conducted by Harley et al. [2013]. The variation of losses in VLD and volute is as expected from the scheme displayed in Figure 5. Skin friction in the diffuser is mostly influenced by the velocity and flow path length in the diffuser and therefore largest at low mass flow rates. The variation of MVD and TVD losses in the volute is associated with the relative lengths of $C_{5,r}$ and $C_{5,u}$ in Figure 5, respectively. Thus, TVD dominates overall volute losses at low mass flow rates and MVD at high mass flow rates.

CONCLUSION

Turbocharger impellers are complex in both, the geometry and the occurring flow phenomena, and state-of-the-art commercial CFD codes are still challenged by the reliable prediction of entire compressor performance maps. Analytical models can therefore be used to investigate the effect of geometrical changes on performance in a preliminary process to narrow down design space before conducting 3D CFD computations to analyse the geometry in detail. The modelling results shall guide the following analysis, as they provide a breakdown of the overall loss to individual mechanisms (Figure 9) which cannot be derived from CFD simulations alone. This information shall help

estimate boundary conditions at different locations, interpret numerical results, explain convergence issues in CFD computations and display the compressor elements with the largest potential for optimisation at a certain operation point.
Single-zone models have a long history of successful application and calibration. They provide robust predictions of performance maps at sufficient accuracy and it is therefore arguable if there is an actual benefit in utilizing the more complex two-zone approach. The modelling of the wake zone requires additional input parameters which influence each other at the risk of numerical instability. However, the more complex a model is, the more detailed are the physical data it can provide. This allows developers to better access interfaces for the incorporation of individual loss mechanisms, especially for mixing loss modelling. Furthermore, developing more complex analytical models supports understanding the interaction of the underlying mechanisms, such as diffusion and blockage in this case. Therefore, the effort of further developing two-zone models does have merit. The presented model shall serve as an alternative to existing approaches and give a framework for the development of sub-models.
The modelling approach is a combination of a two-zone impeller model with 1D loss models. The overall flow model requires a slip model and three physical input parameters, of which the lower border for the wake blockage coefficient $\varepsilon_{2,min}$ was derived from CFD simulations. This parameter accounts for the effect of wake blockage on jet velocity which reduces the diffusion ratio DR towards the choke limit in an iterative procedure. The basic assumption is that choking occurs at the impeller trailing edge and the model relies on the empirical correlation for $\varepsilon_{2,min}(N)$. As this correlation was extracted from CFD results of a single geometry, a major potential for improvement is the investigation of geometrical influencing factors on $\varepsilon_{2,min}$, its transferability to other designs and the derivation of an elaborate model for this parameter.
The benefits of this technique are a smaller dependency on the exact impeller throat area for choke modelling and the off-design diffusion ratio DR which enable a more robust prediction of the choke limit and the overall pressure ratio. Also, considering the interaction of aerodynamic blockage and diffusion rather than both effects in isolation sets the model to a more solid physical basis. At the current state the model does not provide more accurate predictions than single-zone models, however, the large amount of provided data makes it flexible to adaptation and integration of sub-models. Major drawbacks are the dependence on empirical input parameters for initial and boundary values and the validity of assumptions (2 - 4). These have shown to be fully justified only close to the design point in the CFD results. A significant increase of accuracy of the model also requires an improvement of the sub-models for the input parameters.

ACKNOWLEDGEMENT

The authors would like to thank BorgWarner Turbo Systems for the provision of the required compressor geometry and test data and the support in the generation of the presented experimental and numerical results.

REFERENCES

R. H. Aungier. Mean streamline aerodynamic performance analysis of centrifugal compressors. *ASME, Journal of Turbomachinery*, 117(3):360–366, 1995.

N. A. Cumpsty. *Compressor Aerodynamics*. Krieger Publishing Company, Florida, 4th edition, 2004.

R. C. Dean and Y. Senoo. Rotating wakes in vaneless diffusers. *ASME, Journal of Fluids Engineering*, 82(3):563–570, 1960.

S. L. Dixon. *Fluid Mechanics and Thermodynamics of Turbomachinery*. Elsevier Butterworth-Heinemann, Amsterdam, 5th edition, 1998.

M. R. Galvas. Fortran program for predicting off-design performance of centrifugal compressors. NASA, Cleveland, Ohio, 1974. NASA-TN-D-8063.

P. Harley, S. Spence, D. Filsinger, M. Dietrich, and J. Early. Assessing 1D loss models for the off-design performance prediction of automotive turbocharger compressors. In *Proceedings of ASME Turbo Expo 2013: Turbine Technical Conference and Exposition*, San Antonio, USA, 2013.

D. Japikse. A critical evaluation of stall concepts for centrifugal compressors and pumps - studies in component performance, part 7. In *ASME, Stability, Stall and Surge in Compressors and Pumps*, New Orleans, USA, 1984.

D. Japikse. *Centrifugal Compressor Design and Performance*. Concepts ETI, Vermont, USA, 1st edition, 1996.

H. W. Oh, E. S. Yoon, and M. K. Chung. An optimum set of loss models for performance prediction of centrifugal compressors. In *Proceedings of the Institution of Mechanical Engineers, Part A: Journal of Power and Energy*, London, England, 1997.

H. W. Oh., E. S. Yoon, and M. K. Chung. Systematic two-zone modelling for performance prediction of centrifugal compressors. In *Proceedings of the Institution of Mechanical Engineers, Part A: Journal of Power and Energy*, 2002.

J. D. Stanitz. One-dimensional compressible flow in vaneless diffusers of radial- and mixed-flow centrifugal compressors, including effects of friction, heat transfer and area change. NASA, Cleveland, Ohio, 1952. NASA-TN-D-7487.

R. A. van den Braembussche. Centrifugal compressors, analysis and design, 2013. Von Karman Institute for Fluid Dynamics, Course Note 192.

R. A. van den Braembussche, E. Ayder, D. Hagelstein, M. Rautenberg, and R. Keiper. Improved model for the design and analysis of centrifugal compressor volutes. *ASME, Journal of Turbomachinery*, 121(3):619–625, 1999.

C. R. Weber and M. E. Koronowski. Meanline performance prediction for centrifugal compressors. In *ASME Conference Proceedings*, New York, USA, 1986.

F. J. Wiesner. A review of slip factors for centrifugal compressors impellers. *ASME, Journal of Engineering for Power*, 89(4):558–566, 1967.